

Directionality in the *WMAP* Polarization Data

Duncan Hanson¹, Douglas Scott^{1*} and Emory F. Bunn²

¹*Department of Physics & Astronomy, University of British Columbia, Vancouver, B.C. V6T 1Z1, Canada*

²*Physics Department, University of Richmond, Richmond, VA 23173, USA*

Accepted 2007 July 3. Received 2007 June 27; in original form 2007 February 9

ABSTRACT

Polarization is the next frontier of CMB analysis, but its signal is dominated over much of the sky by foregrounds which must be carefully removed. To determine the efficacy of this cleaning it is necessary to have sensitive tests for residual foreground contamination in polarization sky maps. The dominant Galactic foregrounds introduce a large-scale anisotropy on to the sky, so it makes sense to use a statistic sensitive to overall directionality for this purpose. Here we adapt the rapidly computable \mathcal{D} statistic of Bunn and Scott to polarization data, and demonstrate its utility as a foreground monitor by applying it to the low resolution *WMAP* 3-yr sky maps. With a thorough simulation of the maps' noise properties, we find no evidence for contamination in the foreground cleaned sky maps.

Key words: cosmic microwave background – methods: numerical – cosmology: observations – cosmology: theory – large-scale structure

1 INTRODUCTION

Our progress in understanding the large scale make-up of the Universe has been propelled rapidly in the last 15 years by extremely detailed measurements of the Cosmic Microwave Background (CMB). Current measurements of the CMB temperature anisotropies have allowed us to place stringent constraints on some of our Universe's key parameters and are proving to be a driving force in fundamental physics (see e.g. Scott & Smoot 2006). Cosmic-variance places limits on the amount of information which can be extracted from the temperature anisotropies alone, however. The *Planck* satellite, for example, is expected to reach this limit over the entire primary temperature anisotropy power spectrum (*Planck* Bluebook 2006). Fortunately, the polarization of the CMB anisotropies provides us with a wealth of additional cosmological information which we have only just begun to probe. The benefits of CMB polarization data are numerous. Perhaps most excitingly, polarization data provide a chance to detect primordial gravitational waves, through the measurement of B-mode polarization (Seljak & Zaldarriaga 1997; Kamionkowski, Kosowsky & Stebbins 1997; Hu & White 1997; Kamionkowski & Kosowsky 1998). The rapid improvements in CMB polarization data provided by experiments like PIQUE (Hedman et al. 2001), DASI (Kovac et al. 2002), CAPMAP (Barkats et al. 2005), BOOMERanG (Masi et al. 2006), CBI (Readhead et al. 2004), MAXIPOL (Wu et al. 2006), *WMAP* (Page et al. 2006), and upcoming

experiments like BICEP, CLOVER (Taylor 2006), QUAD, and the *Planck* satellite, ensure that polarization will become one of the most important tools we have for furthering our understanding of the Universe in the years to come.

Unfortunately, the polarization signal is much more difficult to measure than the temperature anisotropies. The magnitude of the CMB polarization anisotropies is at most 10 per cent that of the temperature anisotropies, making their detection alone a challenging task. This difficulty is being gradually overcome with improvements in detector technology. Another problem with the CMB polarization, however, is that its signal is dominated over most of the sky by foregrounds. In particular, over the wavelength range where the CMB is typically measured, synchrotron and non-spherical dust emission from within our Galaxy contaminate uncleaned polarization maps. It is not yet clear how well the problem of foreground contamination can be solved. Its resolution will require both a detailed knowledge of the structure and magnitude of the foregrounds, and an understanding of how to remove them from the polarization data without introducing unwanted systematics.

Understandably, the issue of polarization foregrounds has received much attention in the literature. Several papers have been written on the construction of templates for the emission (de Oliveira-Costa et al. 2003; Baccigalupi 2003; Page et al. 2006; Hansen et al. 2006), and a number of methods have been proposed for performing the foreground removal (Bouchet, Prunet & Sethi 1999; Hansen et al. 2006; Slosar, Seljak & Makarov 2004). Testing the efficacy of these methods is a crucial step in the analysis pipeline, to compare the abilities of the various removal techniques and ultimately

* E-mail: dscott@phas.ubc.ca

to provide confidence in the accuracy of CMB polarization data. Tests for the existence of residual polarized foreground contamination have received less attention in the literature, however. The test used in the *WMAP* team's analysis, where foregrounds are cleaned using a template method in pixel space, is a simple χ^2 statistic (Page et al. 2006). Unfortunately, this statistic cannot be used to make comparisons between different cleaning methods. The only currently proposed 'general' statistic which is capable of this application is based on the Bipolar Power Spectrum (BiPS) and has been developed by Basak, Hajian & Souradeep (2006).

In this paper, we introduce and analyse another general method of testing for residual foreground contamination in CMB polarization maps, the \mathcal{D} statistic of Bunn & Scott (2000). It possesses the virtues of having a simple interpretation as a measure of directionality in a CMB map and of being extremely rapid to compute. We argue that this statistic is well suited to the detection of foreground contamination, as both the synchrotron and dust foreground components have strong overall directionality on large scales. We then apply the \mathcal{D} statistic to the *WMAP* 3-yr polarization maps to demonstrate its usefulness for real data.

2 THE \mathcal{D} STATISTIC

The \mathcal{D} statistic was first presented by Bunn & Scott (2000); the \mathcal{D} value for a sky map pixelized into N pixels is defined as

$$\mathcal{D} \equiv \frac{\max_{\hat{n}} f(\hat{n})}{\min_{\hat{n}} f(\hat{n})}, \quad (1)$$

where \hat{n} runs over the unit sphere, and with the function $f(\hat{n})$ given by

$$f(\hat{n}) = \sum_{p=1}^N w_p (\hat{n} \cdot \mathbf{g}_p)^2. \quad (2)$$

Here w_p are weights chosen to compensate for noise and the effects of a cut sky, and \mathbf{g}_p is a local directionality vector calculated for the pixel p . The $f(\hat{n})$ value is a measure of how much (or how little) the \mathbf{g}_p of a map tend to point in a given direction. The \mathcal{D} statistic tells us how extreme these values are. Once \mathcal{D} has been calculated for real sky data, we can compare its value to that found for simulated realizations of the CMB. Calculating \mathcal{D} for a large number of these simulations gives us a histogram of expected values, and excess directionality in a CMB data-set appears as a value of \mathcal{D} which is an outlier of this distribution.

For sky maps of temperature, a reasonable quantity to use for \mathbf{g}_p is the local temperature gradient ∇T_p . For polarization maps, on the other hand, the polarization pseudo-vectors themselves are obvious candidates. We define \mathbf{g}_p to be a vector whose magnitude and direction are those of the polarization at point p . To express \mathbf{g}_p explicitly in terms of the Stokes parameters Q and U , recall that the polarization magnitude is

$$P = \sqrt{Q^2 + U^2}, \quad (3)$$

while the polarization direction lies in the tangent plane to the celestial sphere at p and makes an angle with the meridian of

$$\theta = \frac{1}{2} \tan^{-1} \left(\frac{U}{Q} \right). \quad (4)$$

Measuring the angle from the meridian is a *WMAP* convention (Page et al. 2006) which we adopt here, although it is not universally followed. We define the vector \mathbf{g}_p to have magnitude P and direction given by θ .

Because the polarization is a spin-2 quantity, it is represented by headless 'pseudo-vectors' rather than vectors, so θ can always be rotated by 180° without altering the polarization. However, due to the quadratic definition of $f(\hat{n})$, this ambiguity does not affect \mathcal{D} . Moreover, because the function f smoothly averages together polarization information over the whole sky, \mathcal{D} is only sensitive to large scale ($\gtrsim 20^\circ$) directionality.

The weights w_p must be chosen to satisfy the null hypothesis that for isotropically distributed \mathbf{g}_p no preferred direction will be found on average, even when parts of the sky have been removed. We can see how these weights may be obtained by casting $f(\hat{n})$ in matrix form as

$$f(\hat{n}) = \hat{n}^T \mathbf{A} \hat{n}, \quad (5)$$

where \mathbf{A} is a 3×3 matrix defined by

$$A_{ij} = \sum_{p=1}^N w_p g_{pi} g_{pj}. \quad (6)$$

In order for no preferred direction to be found, we must have $f(\hat{n})$ independent of \hat{n} (on average). From equation 5 it can be seen that this constraint may be realized by choosing suitably normalized w_p such that $\langle \mathbf{A} \rangle$ is equal to the identity matrix for isotropically distributed \mathbf{g}_p . This criterion ensures that $f(\hat{n})$ will be approximately constant over the sky when the underlying data lack a preferred direction, although it does not guarantee that fluctuations of f about its ensemble average will be isotropic. As a result, \mathcal{D} may still pick out preferred directions arising from the noise structure or sky coverage, even when the underlying signal is isotropic. We find that such departures from anisotropy are weak in practice; this point is discussed further in Section 4.

Because \mathbf{A} is symmetric, requiring $\langle \mathbf{A} \rangle = \mathbf{I}$ gives only 6 independent equations on the weights. To completely determine them for a large number of pixels, the additional constraint is imposed that $\text{Var}(w_p P_p)$ be minimized, where P_p is the expected value of $|\mathbf{g}_p|^2$ given by pixel noise and cosmological signal. For a large signal-to-noise ratio on an isotropic sky this is equivalent to minimizing the variance of the weights. When noise is not negligible, minimizing $\text{Var}(w_p P_p)$ rather than $\text{Var}(w_p)$ has the favourable effect of down-weighting noisy pixels. More explicit details on the calculation of the weights are given in Bunn & Scott (2000).

Once the weights w_p have been calculated, the simple quadratic definition of $f(\hat{n})$ makes it possible to calculate \mathcal{D} for a given data-set in $O(N)$ operations, where N is the number of pixels. This can be done by noting that the values of \hat{n} which extremize $f(\hat{n})$ are given by the eigenvectors of \mathbf{A} . \mathcal{D} follows immediately by taking the ratio of the largest and smallest eigenvalues.

\mathcal{D} is one of the simplest statistics which can be proposed for the identification of statistical anisotropy in a CMB map. To compare it to the BiPS method of Basak, Hajian & Souradeep (2006), we note that it is ultimately a less powerful statistic, as BiPS can be used to

probe both large and small scales, whereas \mathcal{D} is only sensitive to large scale anisotropies. The advantage of \mathcal{D} , however, is that it can be calculated in $O(N)$ operations, an unbeatable scaling. This speed makes \mathcal{D} an excellent statistic for ‘first look’ determination of anisotropy in CMB maps, and the concomitant possible foreground contamination.

3 DIRECTIONALITY OF POLARIZATION FOREGROUNDS

The two main sources of foreground contamination in CMB polarization maps at the ~ 100 GHz frequencies where the CMB is usually probed are Galactic synchrotron and thermal dust emission. Polarized synchrotron emission results from the acceleration of cosmic-ray electrons as they orbit in the Galactic magnetic field. Polarized dust emission, on the other hand, is the result of non-spherical dust grains which tend to align their long axes perpendicular to the field; these dust grains preferentially emit thermal radiation polarized along their long axis (Davis & Greenstein 1951).

The polarization of both the synchrotron and thermal dust emission has its origins in the anisotropy introduced by the Galactic magnetic field, and at CMB wavelengths (where Galactic Faraday rotation is negligible) these two components should both be polarized preferentially in the same direction. Thus, we expect that they have a common and distinctive directionality on the sky, dictated by the large scale structure of the Galactic magnetic field. To illustrate the signature of this directionality under application of the \mathcal{D} statistic, we analyse the low resolution K-band polarization map at 23 GHz and the dust polarization template of the WMAP team, masking both with the standard polarization mask (P06) to mimic the situation when analysing maps for foreground contamination. For the K-band map we find a preferred direction at a Galactic latitude 86.4° , within 4° of the poles. For the dust emission template we find that the preferred direction lies at 79.1° , 11° shy of the poles. Thus, the significant presence of synchrotron and dust foregrounds in a polarization map is expected to result in an outlying value of \mathcal{D} , with a preferred direction in the vicinity of the Galactic poles.

4 ANALYSIS OF WMAP 3-YR POLARIZATION DATA

The release of the WMAP 3-year data has provided us with a glimpse at the structure of CMB polarization. Here we analyse the Q and U polarization maps for foreground contamination using the \mathcal{D} statistic.

We have chosen to examine the WMAP low resolution 3rd year (v2) polarization maps¹ at HEALPIX² resolution 4, corresponding to 3072 pixels on the entire sphere. These are the maps used for low ℓ analysis of the WMAP data, corresponding to the angular scales which \mathcal{D} effectively probes. At this resolution it is also feasible to accurately simulate realizations of the WMAP noise structure using the full

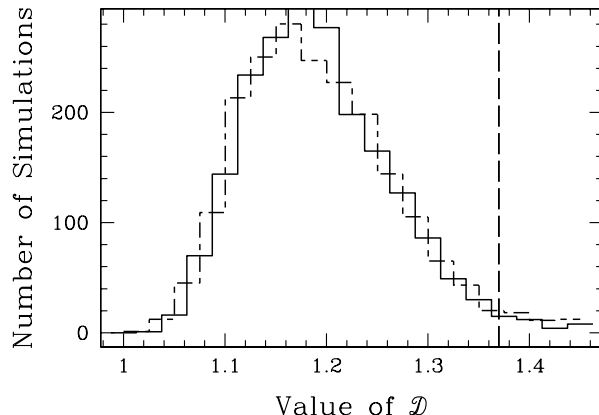


Figure 1. Directionality histograms for maps simulated with WMAP low resolution V-band noise levels, with (solid) and without (dot-dashed) cosmological signal added. The two are essentially indistinguishable. The dashed line shown at $\mathcal{D} = 1.37$ is the value of \mathcal{D} calculated for the V-band data themselves.

noise covariance matrix, which becomes necessary for large angle analyses.

In all of our simulations, we generate cosmological signals given by the ‘WMAP+all Λ CDM’ fit parameters (Spergel et al. 2006). The details of this choice have little effect on the outcome of our simulations. All of the polarization maps are strongly noise-dominated, and we find that histograms of \mathcal{D} for simulated data with and without cosmological signal are indistinguishable for all of the WMAP bands; this is illustrated in Fig. 1 for simulated V-band maps. Thus, we believe that, with an accurate treatment of the maps’ noise properties, any excess directionality which we detect in the WMAP data can be attributed to residual foregrounds, and not a cosmological signal.

For all of our simulations, we add correlated Gaussian noise to each unmasked map pixel based on the *full QU covariance matrices* for the corresponding WMAP frequency band, as provided by the WMAP team. We generate this noise using the Cholesky decomposition of the covariance matrix. This method accounts for QQ, QU and UU correlations both within each pixel and with other pixels across the sky.

For uncleaned maps, the \mathcal{D} statistic produces the expected results. For each band, we generate and analyze ~ 2000 simulated skies. An example of this is shown in Fig. 1. We can use the number of standard deviations (at which the real data lie from the histogram mean) as an approximate measure of the significance with which we detect foreground contamination. This is illustrated in Fig. 2, which shows the expected dependence on radiometer band as the synchrotron emission decreases with frequency and the dust contribution increases, leading to an apparent minimum of foreground contamination near the V-band. We can see that use of the standard P06 polar mask results in a greater level of contamination than when we use the more stringent P02 mask. For the P06 mask, all of the preferred directions which are found for the real data lie within 10° of the Galactic poles, and for the P02 mask the preferred directions all lie within 25° of the poles, further demonstrating the foreground origin

¹ Available at <http://lambda.gsfc.nasa.gov/>

² See <http://healpix.jpl.nasa.gov>

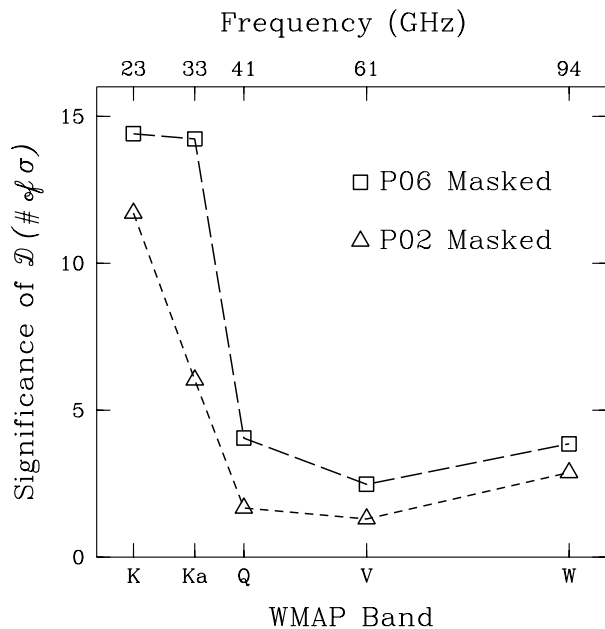


Figure 2. Significances of foreground contamination for the WMAP low resolution maps using noise based on the full covariance matrix. The (\square) symbols are for the standard P06 mask (27 per cent sky cut), while the (\triangle) symbols are for the more stringent P02 masking (50 per cent sky cut for our downgrading scheme). The curve roughly follows that expected from the frequency dependence of contamination by synchrotron and dust foreground components.

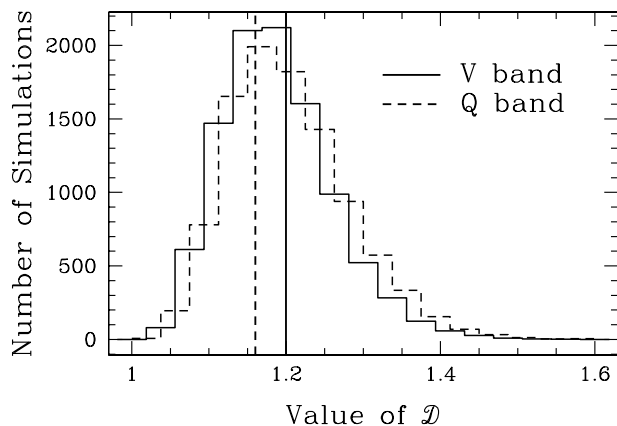


Figure 3. Directionality histograms for simulated realizations of the WMAP V-band (solid) and Q-band (dashed) ‘low resolution foreground reduced’ maps, using the full covariance matrix description of the maps’ noise properties. The vertical lines are the values of \mathcal{D} calculated for the Q- and V-band data themselves.

of the directionality excess. With P06 masking, we find that 98% of our V-band simulations have values of \mathcal{D} less than the value calculated for the WMAP data. With P02 masking, this result drops to 90%. The corresponding significance figures of merit are 2.5σ and 1.3σ respectively.

In order to assess the efficacy of the foreground removal performed by the WMAP team we also analyse the low reso-

lution Q- and V-band foreground reduced maps. These have had dust and synchrotron templates projected out to remove foreground contamination. The results of these analyses are shown in Fig. 3. From this figure it can be seen that the Q and V maps have similar noise properties under analysis with \mathcal{D} , as the simulation histograms almost completely overlap. We find no evidence for residual foreground contamination in these maps, their \mathcal{D} statistics both lying well within the range of probable values, and with the maximal \mathcal{D} directions for the Q- and V-band data being 55° and 27° from the pole, respectively. Our significance figure of merit is 0.6σ for the Q-band and 0.16σ for the V-band maps. 31% of the simulated \mathcal{D} values lie below the map value for the Q-band, and 60% of the simulated data lie below the V-band value. Thus, we find no evidence for foreground contamination in these cleaned maps.

It is interesting to note that if we had generated noise which only accounted for the intra-pixel or diagonal components of the noise covariance matrix then we would have found strong evidence for residual contamination. In the case of the V-band foreground reduced data, for example, we would have found some evidence for foreground contamination, with over 98% of simulated \mathcal{D} values falling below that calculated for real data in the cleaned V-band maps (corresponding to a value of 2.5σ for our significance figure). Accounting for *inter*-pixel noise correlations broadens the distribution of simulated \mathcal{D} values. Indeed, the detailed noise structure of the WMAP data appears to be such that it introduces a degree of anisotropy into the maps. This can best be seen by looking at the histograms of preferred directions found in a series of 30,000 V-band map simulations, given in Fig. 4. Differing methods of noise generation were utilized for three sets of simulations. ‘Diagonal’ noise was generated from only the QQ and UU elements of the covariance matrix, intra-pixel noise included QU terms, and the full covariance matrix treatment simulated inter-pixel correlations as well. Unlike the isotropic distribution of preferred directions which is found when accounting only for diagonal noise correlations, there is a tendency towards anisotropy for the intra-pixel and full covariance simulations, with a definite slight preference for directions in the vicinity of $(l, b) = (150^\circ, 40^\circ)$ for the full covariance simulations. The statistics of these two dimensional histograms support this visual finding, with the diagonal, intrapixel, and full covariance simulation methods having variance/mean values of 1.41, 1.66 and 3.80 respectively. For an isotropic sky, we expect the histogram values to follow a multinomial distribution, and to have a variance/mean of $1 \pm .08$. We believe that the excess variance which is seen in the diagonal and intrapixel simulation histograms can be attributed to the slight inherent bias possessed by \mathcal{D} , as discussed in Section 2. The much higher excess variance seen in the inter-pixel simulations can be attributed to the sum of this bias and another, stronger bias given by the noise covariance structure of the map. This bias is independent of the specifics of the \mathcal{D} statistic, and most likely can be detected in the future by other polarization statistics sensitive to anisotropy. The dependence of our results on the precise treatment of noise underscores the general need for care when dealing with large angle polarization data.

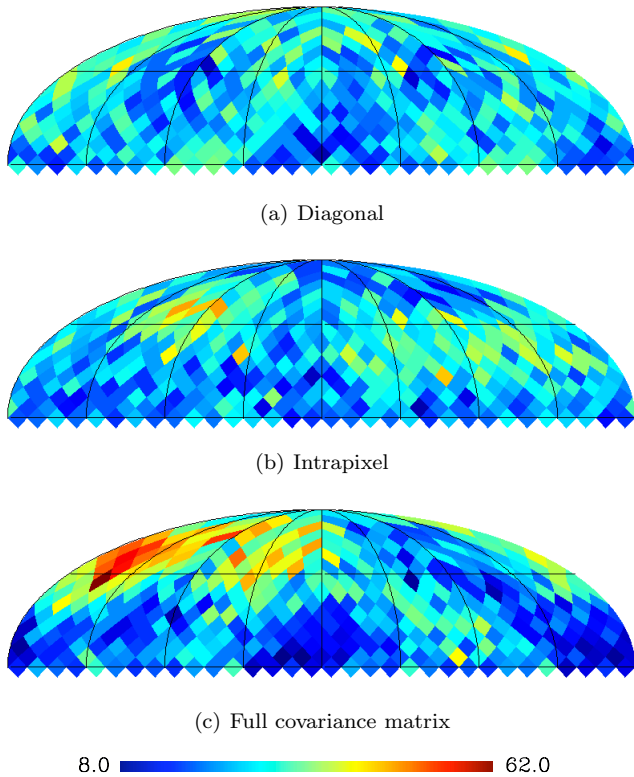


Figure 4. Histograms of preferred direction found for maps simulated with diagonal, intra-pixel, and full covariance matrix based noise (Mollweide projection, Galactic coordinates). The colour units are in number of simulations. The preferred directions calculated by \mathcal{D} are headless, and so we have taken the convention of choosing them to be in the Northern Hemisphere.

5 CONCLUSION

We have investigated the \mathcal{D} statistic of Bunn & Scott (2000) in the context of CMB polarization data, finding that it is an excellent general tool for quickly assessing the magnitude of foreground contamination in polarization maps. Under analysis with \mathcal{D} , imperfectly removed foregrounds leave a tell-tale signature of excess directionality toward the Galactic poles. An analysis of the *WMAP* 3-year polarization data supports these statements. We find the expected dependence of foreground contamination on channel frequency in all of the *WMAP* low resolution maps, with the magnitude of this excess disappearing in the cleaned, ‘foreground reduced’ maps.

In the future, a better understanding of the polarization foregrounds will allow us to develop more sophisticated statistics to precisely evaluate the possibility of foreground contamination in cleaned maps. Given the current state of understanding, however, we feel that calculation of \mathcal{D} is a useful technique for this purpose, as it is one of the simplest possible statistics which captures the directional signature of the polarization foregrounds. It has the advantages of being simple and rapidly computable, and can be considered complementary to other statistics such as the BiPS (Basak, Hajian & Souradeep 2006). Hence it should be one of the diagnostic tests ready to assess foreground contam-

ination in data from the *Planck* satellite, as well as other large-angle polarization experiments.

6 ACKNOWLEDGMENTS

The work carried out in this paper made use of the HEALPIX (Górski et al. 2005) package for pixelization. This research was supported by the Natural Sciences and Engineering Research Council of Canada and the Canadian Space Agency. We also acknowledge the contributions of Patrick Plettner for some related earlier work.

REFERENCES

- Baccigalupi C., 2003, *New Astron. Rev.*, 47, 1127
 Barkats D., et al., 2005, *ApJ*, 619, L127
 Basak S., Hajian A., Souradeep T., 2006, *Phys. Rev. D*, 74, 021301
 Bouchet F.R., Prunet S., Sethi S.K., 1999, *MNRAS*, 302, 663
 Bunn E.F., Scott D., 2000, *MNRAS*, 313, 331
 Davis, L.J., Greenstein, J.L. 1951, *ApJ*, 114, 206
 de Oliveira-Costa A., Tegmark M., O’Dell C., Keating B., Timbie P., Efstathiou G., Smoot G., 2003, *Phys. Rev.*, D68, 083003
 Górski K.M., Hivon E., Banday A.J., Wandelt B.D., Hansen F.K., Reinecke M., Bartelman M., 2005, *ApJ*, 622, 759
 Hansen F.K., Banday A.J., Eriksen H.K., Górski K.M., Lilje P.B., 2006, *ApJ*, 648, 784
 Hedman M., Barkats D., Gundersen J.O., Staggs S.T., Winstein B., 2001, *ApJ*, 548, L111
 Hu, W., White M., 1997, *NewA*, 2, 323
 Kamionkowski M., Kosowsky A., 1998, *Phys. Rev. D*, 57, 685
 Kamionkowski M., Kosowsky A., Stebbins, A., 1997, *Phys. Rev. D*, 55, 7368
 Kovac J., Leitch E.M., Pryke C., Carlstrom J.E., Halverson N.W., Holzappel W.L., 2002, *Nature*, 420, 772
 Masi S., et al., 2006, *A&A*, 458, 687
 Page L., et al., 2007, *ApJS*, 170, 335
Planck BlueBook ‘*The Scientific Programme*’, ESA-SCI(2006)1; astro-ph/0604069v1
 Readhead A.C.S., et al., 2004, *Science*, 306, 836
 Scott D., Smoot, G.F., 2006, in *The Review of Particle Physics*, Yao W.-M., et al., *JPhysG*, 33, 1
 Seljak, U., Zaldarriaga, M., 1997, *Phys. Rev. Lett.*, 78, 2054
 Slosar, A., Seljak, U., Makarov, A., 2004, *Phys. Rev. D*, 69, 123003
 Spergel D.N., et al., 2006, *ApJS*, 170, 377
 Taylor, A., 2006, *NewA Rev.*, 50, 993
 Wu J.H.P., et al., 2007, *ApJ*, 665, 55